Chemical Engineering Journal 99 (2004) 59–68

Chemical Engineering Journal

www.elsevier.com/locate/cej

Effect of hydrodynamics on mass transfer in a gas–liquid oscillatory baffled column

Mónica S.N. Oliveira, Xiong-Wei Ni*

Centre for Oscillatory Baffled Reactor Applications (COBRA), Chemical Engineering, School of Engineering and Physical Sciences, Heriot-Watt University, Riccarton, Edinburgh EH14 4AS, UK

Abstract

In this paper, we present an experimental study on mass transfer of oxygen into water in an oscillatory baffled column (OBC). The objective of this work is to establish the contribution of individual parameters, such as the size of bubbles and the gas holdup, to the overall volumetric mass transfer coefficient (k_La). Our results show that the gas holdup is the most important factor. The liquid-side mass transfer coefficient (k_L) is calculated directly from the experimental measurements of gas holdup, Sauter mean diameter and k_La, and an increase of k_L with D_{32} is observed. The results also show that, above a critical level of fluid oscillation, the mass transfer coefficients are mainly governed by the oscillatory operating conditions, while independent of the type of gas sparger.

Keywords: Fluid oscillation; Mass transfer; Bubble size; Gas holdup; Specific interfacial area

1. Introduction

Gas–liquid contacting is widely used in chemical and biochemical engineering and efficient contacting is essential for promoting gas–liquid mass transfer in chemical and biochemical processes, such as gas–liquid catalytic reactions, fermentation and photosynthesis by micro-organisms. Extensive research on gas–liquid contacting has been undertaken in conventional bubble columns and stirred tank vessels [1–13], and the latter has been the standard device in fermentation industries worldwide. The oscillatory baffled column (OBC) has recently emerged as a viable alternative to those vessels, since it can provide enhanced mass transfer performance [14,15].

The oscillatory baffled column is a mixing technology in which the fluid is oscillated inside a cylindrical tube containing periodically spaced orifice baffles. The flow passing through the baffles induces vortices, which provide significant axial and radial mixing in the column. The intensity of mixing can be controlled by varying the oscillatory (amplitude and frequency) and geometrical (baffle spacing and baffle free area) conditions. It was found that the gas–liquid volumetric mass transfer coefficient in an OBC could be six times higher than that in a bubble column [14] and 75% higher than that in a stirred tank fermenter involving a yeast culture [15].

There are a number of parameters that are directly related to mass transfer, including gas holdup, interfacial area, as well as bubble size and rise velocity. These parameters are complex functions of the physical properties of the gas and liquid phases, the geometry of the vessel used, the gas distributor design, the gas flow rate and other operating conditions. A diagram of the dependencies of these variables, in the context of mass transfer, is shown in Fig. 1.

The complex relations between the parameters require a co-ordinated study into mass transfer in the OBC by considering each of the important parameters independently and collectively. There is, therefore, a clear need to understand the hydrodynamics of gas–liquid interactions within the OBC and to quantify the individual contribution of these parameters to the observed improvement in the mass transfer rates. These are the objectives of this paper.

2. Experimental apparatus

Fig. 2 shows the experimental setup and the main components of the OBC. The dimensions of the column are 50 mm internal diameter (D_C) and 1.5 m height (H_C). The liquid phase volume (V_L) was 2.5 l. The Perspex column was flanged onto a metal table with a supporting structure

* Corresponding author. Tel.: +44-131-451-3781; fax: +44-131-451-3129.
E-mail address: x.ni@hw.ac.uk (X.-W. Ni).

1385-8947/$ – see front matter © 2004 Elsevier B.V. All rights reserved.
doi:10.1016/j.cej.2004.01.002

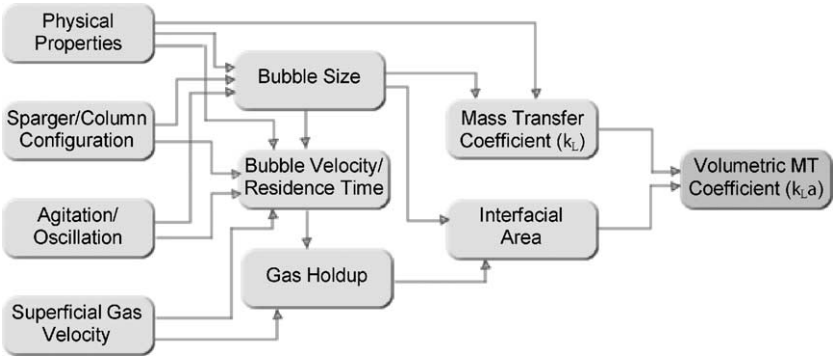

Fig. 1. Diagram showing the dependencies between several variables of a gas–liquid system.

in order to minimise external mechanical vibrations. The open-top column was operated in batch mode at atmospheric pressure and room temperature.

A set of 14 single-orifice baffles, dividing the column into 13 baffled cells, was used in this work. The polytetrafluorethylene (PTFE) baffles were designed to fit closely to the column wall. The geometry of the baffles is also shown in Fig. 2. The baffle thickness (T_b) was 3 mm and the orifice diameter (D_{bo}) was 24 mm, giving a 23% free cross-sectional area (α), which is within the optimal values for mixing [16]. The baffles were supported by four 2 mm diameter stainless steel rods and were equally spaced 75 mm

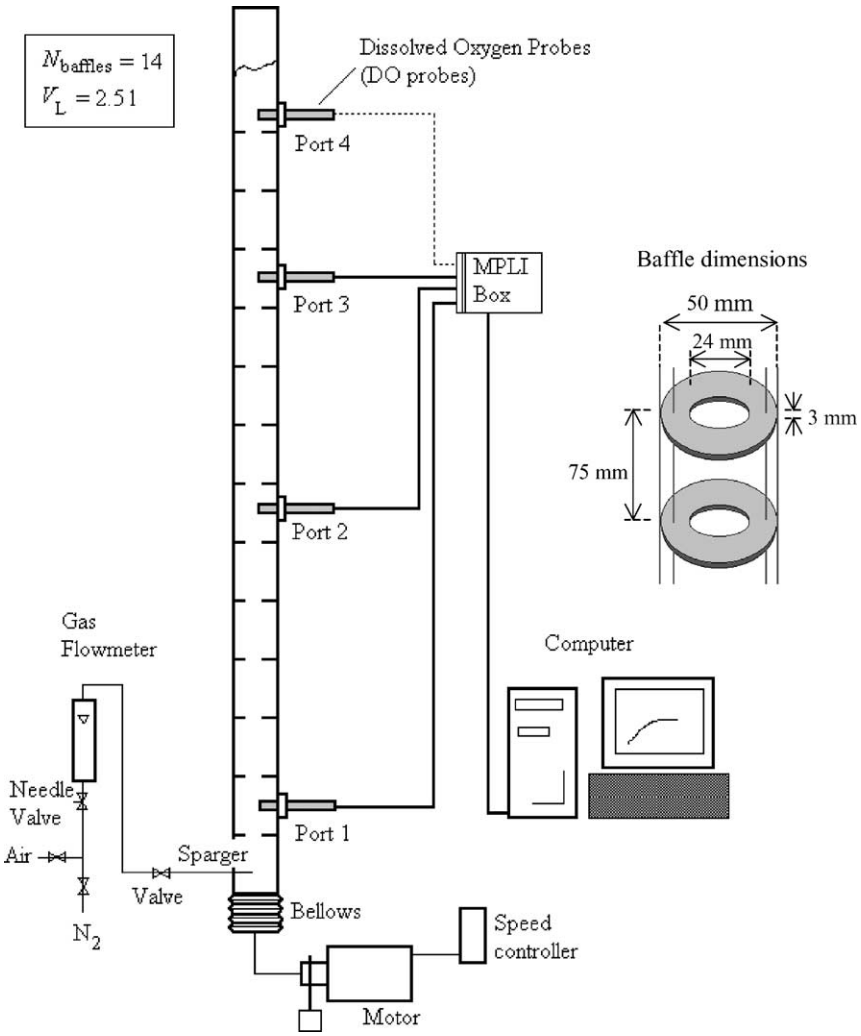

Fig. 2. Schematic representation of the experimental apparatus (not drawn to scale).

Table 1
Conversion between aeration rate and superficial gas velocity

	Aeration rate (vvm) (m^3air/(m^3liquid min))			
	0.05	0.1	0.13	0.2
U_G ($m\,s^{-1}$)	1.06×10^{-3}	2.12×10^{-3}	2.76×10^{-3}	4.24×10^{-3}

apart, corresponding to the optimum baffle spacing (H_b) of 1.5 times the column diameter [17].

The fluid was oscillated by a stainless steel bellows mounted at the base of the column and driven by an electrical motor/gearbox ensemble (Leroy Somer Ltd.) associated with an inverter for speed control (Eurotherm Drives 601). Oscillation frequencies (f) of 0.2–10 Hz could be obtained using the speed controller, and centre to peak oscillation amplitudes (x_0) of 1–10 mm could be selected by adjusting the off-centre (eccentric) position of the connecting rod in the stainless steel coupling wheel.

Gas was continuously fed to the OBC system via a sparger located approximately 40 mm from the base of the column. Two different types of sparger were used: a single-orifice sparger of 1 mm diameter (sparger 1) and a porous borosilicate glass sparger (sparger 2). At low gas flow rates in stagnant water, the single-orifice sparger generates a series of medium sized bubbles, while the porous glass sparger supplies a school of small bubbles. The gas flow rate was controlled by a needle valve and measured by a calibrated flowmeter. Aeration rates ranging from 0.05 to 0.2 vvm were used in this work, where vvm is the volume of air per volume of liquid per minute, and has a unit of m^3 air/(m^3 liquid min). Table 1 shows the conversion between the aeration rates expressed in terms of vvm and the superficial gas velocities (U_G = vvm $\times$ V_L/A_C), where A_C stands for the column cross-sectional area.

The dynamic gassing out method with instantaneous gas interchange was employed to determine the mass transfer coefficient. This method has been used in several types of vessels, including OBCs [18]. The experimental procedure was as follows. Firstly, the liquid was deoxygenated by gassing nitrogen through the column. The gas supply was then switched from pure nitrogen to air, whilst maintaining a constant gas flow rate. During the whole process, the fluid was oscillated continuously at the selected frequency and amplitude. The dissolved oxygen (DO) concentration was measured using three Clark-type polarographic DO probes positioned axially along the column. Ports for the DO probes were located at cells numbered 2, 7, 11 and 14, as shown in Fig. 2. The signal outputs from the DO probes were continuously monitored and recorded on a computer via a multi-purpose lab interface (MPLI). It should be noted that this interface box could only lodge three inputs at one time. Consequently, only three probes were used during each individual measurement.

Prior to usage, DO probes were filled with the potassium chloride electrolyte supplied by the manufacturer, were allowed to polarise for 1 h and were then calibrated. The electrodes automatically compensated for temperature variations. It should be emphasised that the calibration of the DO probes is not strictly necessary, since the calculated values of the mass transfer coefficient can be shown to be independent of the calibration procedure [19]. The general form of the probe response is

$$C_P\,(\mathrm{mol\,m^{-3}}) = C_L^* - (C_L^* - C_{L_0})\,f(t) \quad (1)$$

where C_P is the DO concentration read by the probe ($mol\,m^{-3}$), C_L^* the DO concentration in the liquid phase in equilibrium with the gas phase ($mol\,m^{-3}$), C_{L_0} the DO concentration in the liquid phase ($mol\,m^{-3}$) at time $t = 0$, and $f(t)$ represents a generic function of time. The calibration process simply relates the output of the probe (E) to the actual oxygen concentration by a linear relationship:

$$C = EK_{calib} \quad (2)$$

where K_{calib} is the calibration constant. Substitution of Eq. (2) into Eq. (1) yields

$$E_P = E_L^* - (E_L^* - E_{L_0})\,f(t) \quad (3)$$

since the calibration constants on both sides of the equation cancel out. Thus, the mass transfer coefficient calculated from the fit to a given response curve will always be the same, regardless of the calibration.

Fig. 3 shows a typical profile of the dissolved oxygen concentration in the liquid as a function of time. A noticeable delay was observed in most profiles, even for measurements at port 1, located near the bottom of the column, as illustrated in Fig. 2. This delay was due to the length of tubing between the Air/N_2 valves and the sparger (Fig. 2), due to the probe response delay and due to the effect of gas and liquid dynamics in the column. In fact, the time delays were different for different probe locations along the column. For this reason, a floating co-ordinate ($t - t_0$) was used in the analysis, with the delay time (t_0) as a fitting parameter.

The calculation of k_La involved fitting a mass balance equation to each experimentally measured DO concentration curve. The mass balance equation was obtained from a

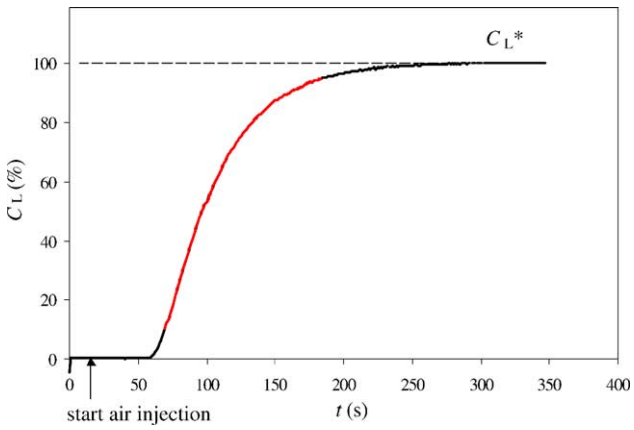

Fig. 3. Typical experimental DO concentration profile. For the calculation of k_La, only the points of C_L between 70 and 190s were considered.

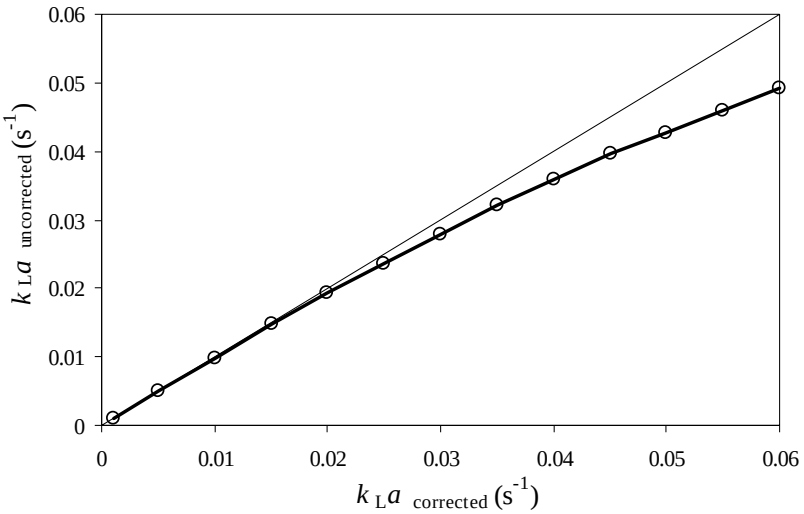

Fig. 4. Uncorrected vs. corrected $k_L a$ values. The thin solid line represents $y = x$.

model of the dynamic behaviour of the physical system. Several factors, such as the start-up period, nitrogen transport, gas and liquid mixing and probe dynamics were examined. The effects of the first two factors on $k_L a$ were considered to be negligible when an immediate interchange of feed between nitrogen and air, at a constant flow rate, was adopted [20–22].

The state of mixing in either the gas or the liquid phase can affect the determination of $k_L a$. Several models, e.g. steady-state, perfect mixing and tanks-in-series, can be used to account for different degrees of mixing. Some of these models were compared, and it was found that a reliable mass transfer coefficient could be calculated using the steady-state model [19]. The effects of the gas and liquid dynamics are mainly visible at the low end of the DO response, e.g. <10% of C_L^*. Furthermore, when the DO concentration is above approximately 95%, the electrode is not very sensitive to small changes in the DO concentration. For these reasons, truncation of the DO response was employed in the determination of $k_L a$, and DO concentrations less than 10% and greater than 95% of C_L^* were discarded (Fig. 3), so as to increase the accuracy and minimise the influence aforementioned.

As for the probe dynamics, it was found that a first order model was appropriate to describe the response of all the probes used [19]. Measurements of probe responses to step changes in concentration were carried out frequently throughout the course of the mass transfer experiments, using the procedure detailed in Oliveira [19]. The probe constants (k_P) showed a high degree of repeatability and, as such, a reliable average k_P for probes in ports 1–3 was determined as $0.148 \pm 6.1 \times 10^{-3}$, $0.112 \pm 7.4 \times 10^{-3}$ and $0.137 \pm 6.1 \times 10^{-3}\,s^{-1}$, respectively.

Combining a steady-state model for the gas dynamics and a perfectly mixed liquid phase, together with a first order probe response, $k_L a$ can be calculated by fitting the experimental DO concentration profile to Eq. (4), with time as a floating co-ordinate:

$$C_L = C_L^* - \frac{C_L^* - C_{L_0}}{k_L a - k_P}\{k_L a \exp[-k_P(t - t_0)] - k_P \exp[-k_L a(t - t_0)]\} \quad (4)$$

The effect of the probe delay on $k_L a$ is shown in Fig. 4. The corrected $k_L a$ values were obtained from Eq. (4), while the uncorrected values were calculated using Eq. (5), which ignores the probe delay:

$$C_L = C_L^* - (C_L^* - C_{L_0}) \exp[-k_L a(t - t_0)] \quad (5)$$

The lowest probe constant, $k_P = 0.112\,s^{-1}$ was used in the calculations in Fig. 4, reflecting the case where the influence of the probe delay in $k_L a$ is the greatest. It is clear that for values of $k_L a$ lower than $0.02\,s^{-1}$, the probe dynamics had no significant influence, while for values greater than $0.02\,s^{-1}$, the correction for the probe delay had to be taken into account. In light of this finding, $k_L a$ was determined by using Eq. (4) in all subsequent calculations. The procedure of fitting the DO profiles to this equation was implemented in *Matlab*, using $k_L a$ and t_0 as fitting parameters. The full range of conditions for which the mass transfer coefficients were measured is shown in Table 2.

Table 2
Range of operational variables

x_0 (mm)	f (Hz)	Re_0	St	vvm
0	0	0	–	0.05–0.2
2	1–8	624–4993	2.0	0.05–0.2
4	1–8	1248–9985	1.0	0.05–0.2
8	1–5	2496–12481	0.5	0.05–0.2

3. Results and discussion

Experimental mass transfer results in the OBC are shown in this section for several operating conditions. The values

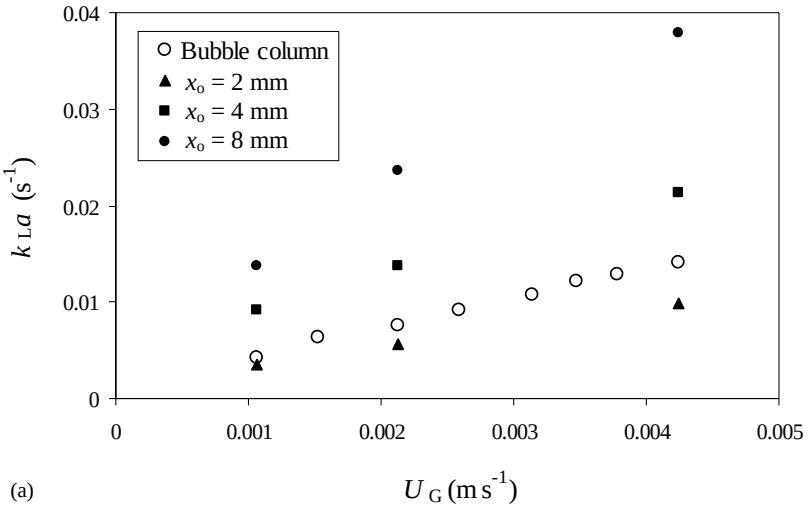

Fig. 5. Mass transfer coefficient as a function of superficial gas velocity in the OBC with the porous sparger: (a) for a fixed oscillation frequency, $f = 5$ Hz; (b) for a fixed oscillation amplitude, $x_0 = 4$ mm.

of k_La with the porous sparger are plotted as a function of the superficial gas velocity, for different oscillation amplitudes at a fixed frequency (Fig. 5a) and for different frequencies at a fixed amplitude (Fig. 5b). It can be seen that, in all cases, k_La increases with U_G, as well as with either oscillation frequency or amplitude. These figures also show the corresponding results for the bubble column, i.e. the same column without baffles and oscillation. The important thing to note is that, when the column is fitted with the porous sparger, it is possible to enhance mass transfer by applying oscillation in the presence of baffles. For the range of aeration rates studied, improved mass transfer coefficients are obtained for oscillation levels above, e.g. $x_0 = 4$ mm and $f = 4$ Hz (Fig. 5). At the highest oscillation levels employed in this work, the values of k_La in the OBC are about four times higher than in the bubble column. When the column is fitted with the single-orifice sparger, the improvement in mass transfer in the OBC is even more significant, and k_La can be increased by a factor of 13.

The effects of oscillation frequency and amplitude on k_La for the porous sparger are plotted in Fig. 6 as a function of frequency for different amplitudes and aeration rates. An increase in the frequency leads to an increase in the k_La. The increase is small initially, but becomes more pronounced at higher oscillation frequencies, in accordance with the effect of oscillation on gas holdup [23]. The trends and magnitudes of k_La shown here are in accordance to previous mass transfer studies in OBCs [14,18,24]. Fig. 7 compares the values of k_La at the same operating conditions for the two different spargers. The results are essentially indistinguishable within experimental error. This is surprising, given the fact that the bubble dispersions produced by each sparger in the absence of oscillation and baffles are significantly different. The almost identical k_La values for the two spargers

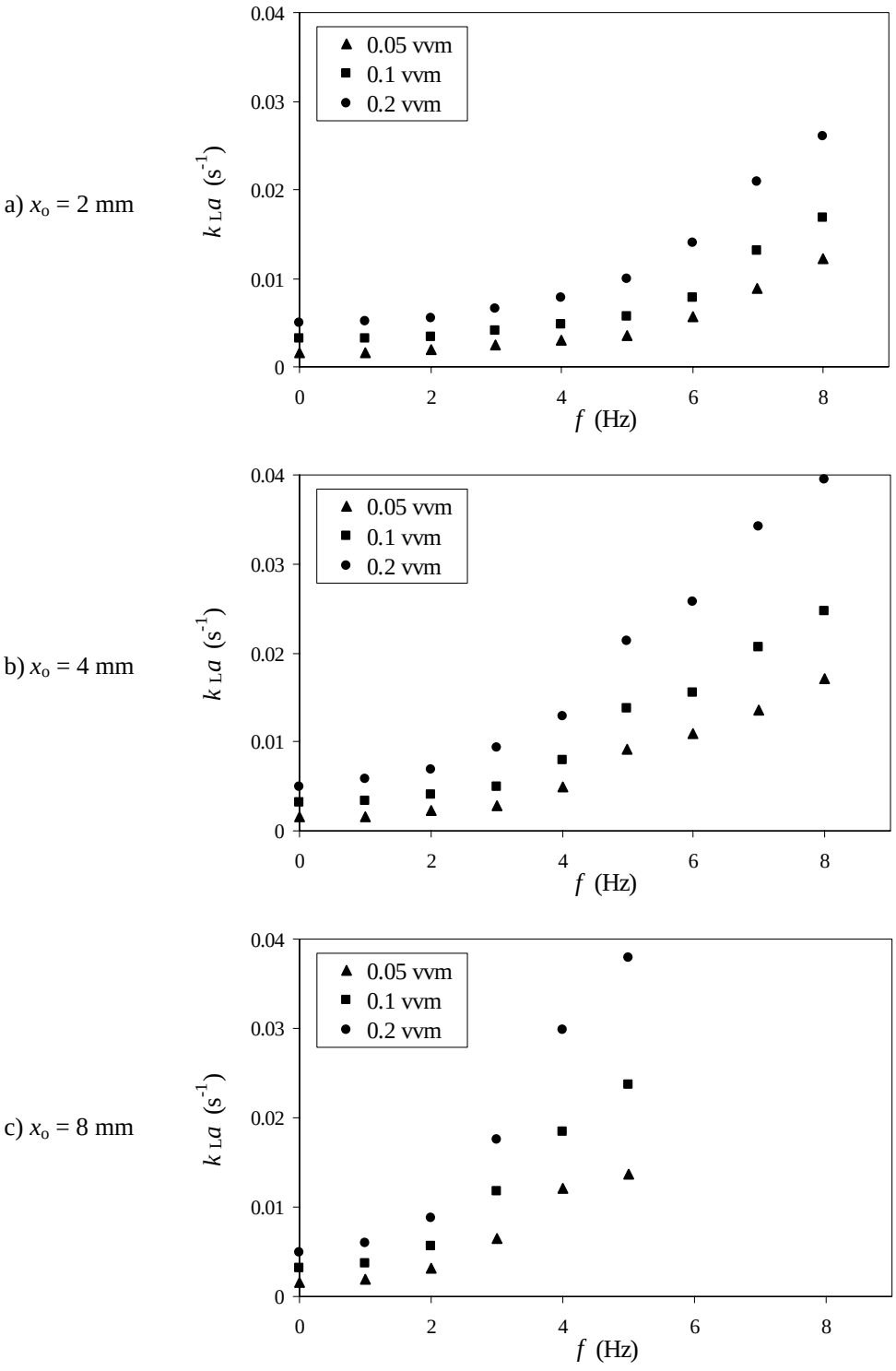

Fig. 6. Effect of oscillation frequency on k_La in the OBC with the porous sparger.

are a result of the high turbulence generated by the fluid oscillation. Under fluid oscillation, mass transfer is dominated by the fluid flow patterns, and is independent of the type of gas distributor. It can also be observed from Fig. 7 that the increase in the slope of k_La versus oscillation frequency occurs earlier for higher amplitudes. Essentially, the slopes are shifted to lower frequencies as the amplitude increases. This suggests that, as in the case of the gas holdup, it is the combined effect of oscillation frequency and amplitude that is responsible for the enhancement of mass transfer.

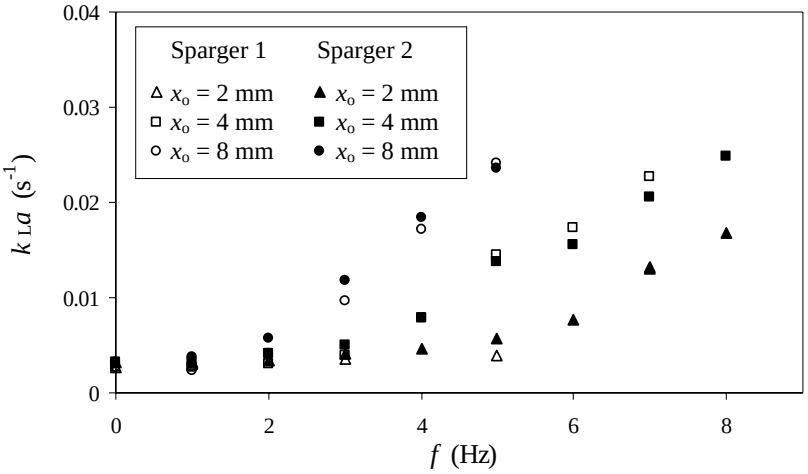

Fig. 7. Mass transfer coefficient vs. frequency in the OBC (0.1 vvm).

In summary, the overall mass transfer coefficient in the OBC increases significantly with both oscillation frequency and amplitude. This is a consequence of the highly turbulent flow pattern generated in the column as the oscillation increases, leading to frequent bubble breakage and a subsequent reduction in the Sauter mean diameter, as well as an increase in the residence time of the bubbles, when trapped in recirculating vortices [23].

The experimental measurements presented here suggest that the volumetric mass transfer coefficient depends on hydrodynamic parameters, such as the bubble size and the gas holdup (which is directly related to the residence time of the gas phase). To establish the relative importance of each of these factors, k_La was correlated as a function of Sauter mean diameter (D_{32}) and holdup (ε_G) measured experimentally [19,23] using a least-squares method. The resulting expression (including 95% confidence levels on the exponents) is

$$k_La\,(\text{SI units}) = 0.043\frac{\varepsilon_G^{1.0\pm0.07}}{D_{32}^{0.45\pm0.11}} \quad (6)$$

According to Eq. (6), the volumetric mass transfer coefficient is influenced by both an increase in the gas holdup, due to a prolonged residence time of the gas phase, and a decrease in the Sauter mean diameter. It is the combination of these two effects that brings about the substantial enhancement of mass transfer in the OBC, compared to a bubble column, as observed here and in previous studies [14]. Furthermore, it is seen that the influence of gas holdup on k_La is stronger than that of bubble size. This is in qualitative agreement with our previous study [25], although the values of the exponents are slightly different. The discrepancy can be attributed to the fact that the previous analysis was performed using empirical correlations based on experimental data obtained in different geometrical and operating conditions. Fig. 8 shows the fit to k_La data using Eq. (6), for a given set of operating conditions, and clearly the agreement is very good. In fact, Eq. (6) is able to correlate the volumetric mass transfer coefficients quite accurately over the entire range of experimental conditions, as shown in Fig. 9. The average relative error of the fit is 13%.

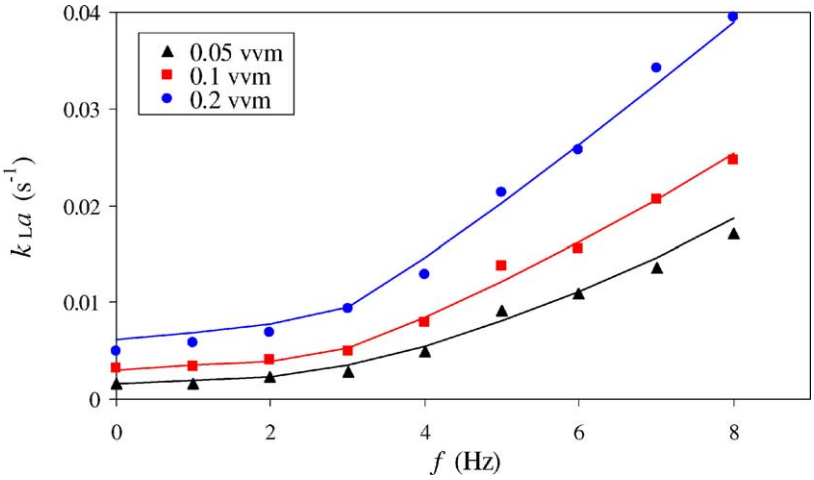

Fig. 8. Comparison of the volumetric mass transfer coefficient obtained experimentally (symbols) and calculated using Eq. (6) (solid lines) ($x_0 = 4$ mm).

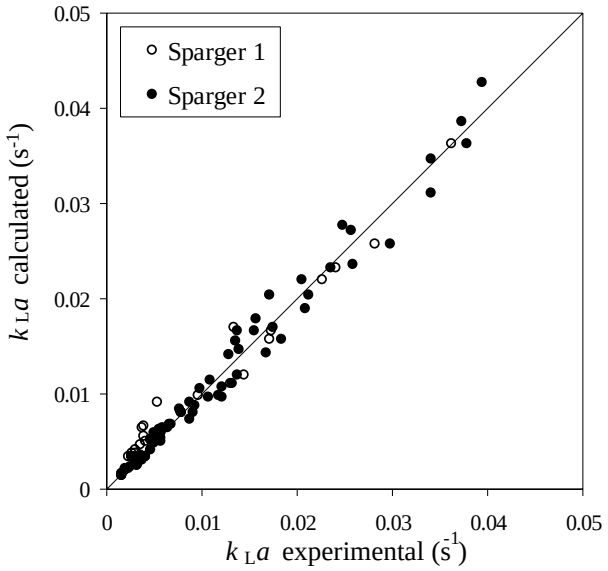

Fig. 9. Comparison of the volumetric mass transfer coefficient obtained experimentally and calculated using Eq. (6). The solid line represents $y = x$.

The specific interfacial area available for mass transfer (a) can be estimated from the following equation:

$$a = \frac{6\varepsilon_G}{D_{32}} \tag{7}$$

Combining this equation with k_La data, it is possible to evaluate the liquid-side mass transfer coefficient (k_L), according to

$$k_L\ (\mathrm{m\,s^{-1}}) = \frac{(k_La)D_{32}}{6\varepsilon_G} \tag{8}$$

Fig. 10 shows a plot of k_L in the OBC as a function of the Sauter mean diameter. The first observation is that the values of k_L exhibit a high degree of scattering. This is due to the fact that the calculation of k_L from Eq. (8) accumulates three different experimental errors, in the measurements of k_La, D_{32} and ε_G. In spite of this, a general increasing trend of the liquid-side transfer coefficient with the bubble size is observed.

A similar increase in k_L with the Sauter mean diameter has been observed previously, from mass transfer measurements in stirred tanks [26,27], bubble columns [28,29], reciprocating-plate columns [30,31] and pulsed columns [32]. Calderbank [33] suggested the existence of two bubble size ranges ("small" and "large"), within which the values of k_L are essentially independent of bubble size and are controlled by the turbulence of the liquid phase [34]. When the bubbles are small, they behave as rigid spheres, with practically no fluid circulation at the surface. In this regime, theoretical equations based on flow around rigid spheres are valid [33], and k_L is proportional to $D_L^{2/3}$, where D_L is the gas diffusivity ($\mathrm{m^2\,s^{-1}}$). Large bubbles, on the other hand, have mobile interfaces and exhibit significant fluid circulation. In this case, theories based on the renewal of the liquid film at the interface, such as Higbie's penetration theory [35] or Danckwerts' surface renewal theory [36], are applicable [26]. For large bubbles, the liquid-side mass transfer coefficient is a function of $D_L^{1/2}$. As a result of the differences in fluid circulation at the surface, the values of k_L for large bubbles are substantially higher than those for small bubbles, with a transition region in between characterised by a steep increase in k_L [26].

In the transition region, the liquid-side mass transfer coefficient is controlled by the bubble diameter [30]. Other effects of increasing the agitation of the continuous phase, leading to a possible increase in the renewal rate of the liquid film at the interface, are probably of secondary importance and are masked by the predominant effect of a decrease in the bubble diameter. Montes et al. [37] have demonstrated from theoretical considerations that the observed increase in k_L with bubble size in the transition region is due to a gradual increase in the amplitude of shape oscillations of the

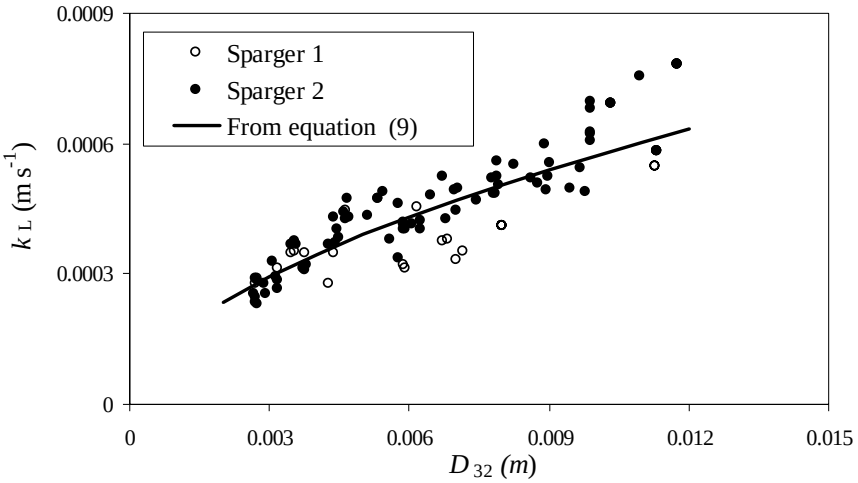

Fig. 10. Effect of Sauter mean diameter on k_L calculated using Eq. (8).

bubbles. Although Calderbank and Moo-Young [26] located this transition region at diameters of approximately 2–3 mm, subsequent studies [28,30,31] showed that k_L may increase with D_{32} for a much wider range of bubble diameters (from 1.7 to 8 mm). The location of the transition region is highly dependent on the characteristics of the system, in particular on the purity of the liquid phase [38,39]. Variations of k_L with D_{32} [26,31,32], $D_{32}^{0.813}$ [27] and $D_{32}^{1/2}$ [28] have been proposed. By substituting Eq. (6) into Eq. (8), an expression for the relative dependence of k_L on D_{32} in the OBC was obtained:

$$k_L \text{ (SI units)} = 0.0072 D_{32}^{0.55\pm0.11} \quad (9)$$

This equation is shown as the solid line in Fig. 10. The exponent of 0.55 obtained in this work, agrees, within statistical limits, with the results of Akita and Yoshida [28]. However, it should be noted that this type of analysis must be interpreted with caution, due to the large scatter in the k_L data (both in this work and in the studies aforementioned).

As reported previously, the turbulent nature of the flow in the OBC causes bubbles to break, and a consequent decrease in the Sauter mean diameter. This leads to an increase in the gas–liquid interfacial area, which is advantageous for mass transfer. However, this effect is counterbalanced by a decrease in k_L with decreasing D_{32}, due to the reduced mobility of the surface of the bubbles (as explained above). The overall result of this is that the effect of bubble size on k_La is not as strong as that of gas holdup (Eq. (6)).

4. Conclusions

This paper has shown that the volumetric mass transfer coefficient increases with the aeration rate, both in a bubble column and in an OBC. The volumetric mass transfer coefficient increased considerably with both oscillation frequency and amplitude. Furthermore, it was observed that k_La in the OBC was independent of the sparger type, and was instead mainly governed by the turbulent flow patterns in the column. Significantly higher values of k_La were observed in the OBC than in the bubble column, even for relatively low oscillation intensities. This was true even when the column was fitted with a porous sparger, which is designed to produce high gas–liquid interfacial areas. These improvements are extremely important in applications, such as fermentation, that involve mass transfer of a sparingly soluble solute (e.g. oxygen) into the liquid phase, and where this is the rate-controlling step [40,41].

The individual effects of bubble size and gas holdup on mass transfer in an OBC were evaluated, by correlating k_La as a function of these two parameters. The expression obtained provided an accurate representation of the experimental data over the whole range of operating conditions studied. The simultaneous increase in the gas holdup caused by an increase in the residence time of bubbles that become trapped in vortices, and the decrease in the Sauter mean diameter due to the action of turbulent eddies, results in a substantial increase in the gas–liquid interfacial area of the dispersion. However, the decrease in the bubble size causes the bubbles to become more rigid, with less fluid circulation at the interface, and this implies a reduction in the liquid-side mass transfer coefficient. This effect is outweighed by the observed increase in the interfacial area. As a direct consequence of these opposite effects, the Sauter mean diameter plays a much less important part in the enhancement of mass transfer than the gas holdup.

The combined measurements of ε_G, D_{32} and k_La allowed for the calculation of the liquid-side mass transfer coefficient. It is the first time that such calculations have been presented for an OBC. It was observed that k_L increased with the bubble diameter, due to an decrease in the rigidity of the gas–liquid interface, which is in accordance with previous observations in other types of gas–liquid contacting devices. Further research would be necessary to gain knowledge of the effect of oscillation on the liquid-side mass transfer coefficient over a wider range of operating conditions. This would help separate the effect of fluid agitation on the renewal of the interfacial liquid film from the effect of increased surface rigidity, brought about by bubble breakage. A refinement of the experimental methods would also be advantageous, so as to reduce the amount of error affecting the calculation of k_L.

Acknowledgements

M.S.N. Oliveira wishes to acknowledge Fundação para a Ciência e Tecnologia and Heriot-Watt University for financial support.

References

[1] P.H. Calderbank, Trans. IChemE 36 (1958) 443.
[2] R. Shinnar, J. Fluid Mech. 10 (1961) 259.
[3] F.B. Sprow, AIChE J. 13 (1967) 995.
[4] R.L. Panton, A.L. Goldman, J. Acoustic Soc. Am. 60 (1976) 1390.
[5] P.F. Tooby, G.L. Wick, J.D. Isaacs, J. Geophys. Res. 82 (1977) 2096.
[6] S.M. Bhavaraju, T.W.F. Russel, H.W. Blanch, AIChE J. 24 (1978) 454.
[7] R. Clift, J.R. Grace, M.E. Weber, Bubbles, Drops and Particles, Academic Press, New York, 1978.
[8] K.D. Stephanoff, I.J. Sobey, B.J. Bellhouse, J. Fluid Mech. 96 (1980) 27.
[9] R.M. Thomas, Int. J. Multiphase Flow 7 (1981) 709.
[10] W. Zakrzewski, J. Lippert, A. Lübbert, K. Schügerl, Eur. J. Appl. Microbiol. Biotechnol. 12 (1981) 150.
[11] K.J. Sene, J.C.R. Hunt, N.H. Thomas, J. Fluid Mech. 259 (1994) 219.
[12] C. Tsouris, L.L. Tavlarides, AIChE J. 40 (1994) 395.
[13] R. Parthasarathy, N. Ahmed, J. Chem. Eng. Jpn. 29 (1996) 1030.
[14] M.R. Hewgill, M.R. Mackley, A.B. Pandit, S.S. Pannu, Chem. Eng. Sci. 48 (1993) 799.
[15] X. Ni, S. Gao, R.H. Cumming, D.W. Pritchard, Chem. Eng. Sci. 50 (1995) 2127.

[16] X. Ni, G. Brogan, A. Struthers, D.C. Bennet, S.F. Wilson, Trans. IChemE 76 (1998) 635.
[17] C.R. Brunold, J.C.B. Hunns, M.R. Mackley, J.W. Thompson, Chem. Eng. Sci. 44 (1989) 1227.
[18] X. Ni, S. Gao, J. Chem. Technol. Biotechnol. 65 (1996a) 65.
[19] M.S.N. Oliveira, Characterisation of a gas–liquid oscillatory baffled column, PhD Thesis, School of Engineering and Physical Sciences, Chemical Engineering, Heriot-Watt University, Edinburgh, UK, 2003.
[20] I.J. Dunn, A. Einsele, J. Appl. Chem. Biotechnol. 25 (1975) 707.
[21] V. Linek, P. Benes, F. Hovorka, Biotechnol. Bioeng. 23 (1981) 301.
[22] V. Linek, P. Benes, V. Vacek, F. Hovorka, Chem. Eng. J. Biochem. Eng. J. 25 (1982) 77.
[23] M.S.N. Oliveira, X. Ni, AIChE J., submitted for publication.
[24] X. Ni, S. Gao, Chem. Eng. J. 63 (1996) 157.
[25] M.S.N. Oliveira, X. Ni, Chem. Eng. Sci. 56 (2001) 6143.
[26] P.H. Calderbank, M.B. Moo-Young, Chem. Eng. Sci. 16 (1961) 39.
[27] C.W. Robinson, C.R. Wilke, AIChE J. 20 (1974) 285.
[28] K. Akita, F. Yoshida, Ind. Eng. Chem. Process Des. Dev. 13 (1974) 84.
[29] J.J. Heijnen, K. Van't Riet, Chem. Eng. J. 28 (1984) B21.
[30] K. Miyanami, K. Tojo, I. Minami, T. Yano, Chem. Eng. Sci. 33 (1978) 601.
[31] V. Veljkovic, D. Skala, Can. J. Chem. Eng. 66 (1988) 200.
[32] M.H.I. Baird, J.H. Garstang, Chem. Eng. Sci. 27 (1972) 823.
[33] P.H. Calderbank, Trans. IChemE 37 (1959) 173.
[34] J.C. Lamont, D.S. Scott, AIChE J. 16 (1970) 513.
[35] R. Higbie, Trans. AIChE 31 (1935) 365.
[36] P.V. Danckwerts, Ind. Eng. Chem. 43 (1951) 1460.
[37] F.J. Montes, M.A. Galan, R.L. Cerro, Chem. Eng. Sci. 54 (1999) 3127.
[38] S. Sideman, O. Hortacsu, J.W. Fulton, Ind. Eng. Chem. 68 (1966) 32.
[39] V. Linek, J. Mayrhoferová, J. Mošnerová, Chem. Eng. Sci. 25 (1970) 1033.
[40] H.H. Topiwala, G. Hamer, Trans. IChemE 52 (1974) 113.
[41] M.Y. Chisti, Airlift Bioreactors, Elsevier, Amsterdam, 1989.